JARO 02: 257–267 (2001)
DOI: 10.1007/s101620010013

JARO
Journal of the Association for Research in Otolaryngology

Longitudinal Coupling in the Basilar Membrane

RAM C. NAIDU[1,2] AND DAVID C. MOUNTAIN[1–3]

[1]*Hearing Research Center, Boston University, Boston MA, 02215, USA*
[2]*Department of Biomedical Engineering, Boston University, Boston MA, 02215, USA*
[3]*Department of Otolaryngology, Boston University, Boston, MA 02215, USA*

Received: 27 December 1999; Accepted: 29 March 2001; Online publication: 17 May 2001

ABSTRACT

A systematic and detailed study of the longitudinal coupling exhibited by the basilar membrane (BM) was performed in the excised gerbil cochlea. Contrary to the notion that the adjacent regions of the BM are decoupled from each other, the data indicate that: (a) the BM exhibits longitudinal coupling; (b) the length of the coupled region increases from base to apex of the cochlea; and (c) the cells of the organ of Corti (OC) increase the overall coupling exhibited by the BM. Modeling results show that, at a given location, longitudinal coupling increases the effective stiffness of the OC near the characteristic frequency. Therefore, the effect of longitudinal coupling cannot be neglected in the region of the peak of the traveling wave.

Keywords: basilar membrane, longitudinal coupling, cochlea

INTRODUCTION

Sound reaching the external ear induces motion along the sensory epithelium within the cochlea. The auditory transduction process relies upon specific details of this motion to generate an accurate neural representation of the sound stimulus. The organ of Corti (OC) and the underlying basilar membrane (BM) compose the sensory epithelium, and their mechanical properties interact together to determine its composite motion in response to sound. In order to understand how the epithelium moves, it is necessary to determine whether the motion at a single location on the BM is influenced by motion at other locations along the length of the BM. In cochlear mechanics parlance, this is equivalent to determining whether the BM is "longitudinally coupled" or "longitudinally decoupled."

Typically, models of the cochlea assume that the BM is longitudinally decoupled. The BM can then be divided into numerous thin radial segments that move independently of each other [see de Boer (1997) for review]. Mathematically, the decoupled BM is extremely attractive since it allows the equations that describe the motion of a single section of the BM to be independent of the equations that describe the motion of other sections along its length. The propagation of energy from section to section as the traveling wave progresses through the cochlea, can occur only through fluid movement in the scalae above and below the OC. Alternately, if the BM is significantly coupled, the motion at a given location can potentially influence the motion of other regions along the length of the BM. Some of the energy traveling through the cochlea could then be transmitted along the BM as well. Allen and Sondhi (1979) reported that the inclusion of longitudinal coupling in their model introduced undesirable high-frequency characteristics in the predicted response. On the other hand, Wickesberg and Geisler (1986) showed that longitudinal coupling had favorable effects on their model and caused a broadening of the otherwise narrow peak of the predicted BM displacement.

Previous studies (von Békésy 1960; Voldřich 1978) have provided contradictory descriptions of the longitudinal coupling exhibited by the BM. The results of these studies were described qualitatively, based on visual observation through the microscope. We first

Correspondence to: Dr. Ram C. Naidu · Department of Biomedical Engineering · Boston University · 44 Cummington Street · Boston, MA 02215. Telephone: (617) 353-9149; fax: (617) 353-6766; email: cram@bu.edu

cite the results of von Békésy (1960). Von Békésy removed the cells of the OC and deflected the BM with a blunt probe. He observed that this local deflection elicited deflections over an extended region of the cochlear turn. Furthermore, he described the shape of the resulting deformation in the BM to be circular near the cochlear apex and elliptical near the stapes, with the longer axis of the ellipse oriented along the length of the BM. These results, which indicated significant longitudinal coupling in the BM, were obtained from experiments that were performed in the cochleae of cadavers. It is, therefore, unclear as to whether these results can be extended to the living cochlea which deteriorates rapidly when its natural environment is compromised (Rhode 1973).

A second study was performed by Voldřich (1978) in a manner similar to that described by von Békésy (1960). The experiments were once again performed on the BM with the OC removed, but this time in preparations of the freshly excised guinea pig cochlea. Voldřich described the BM deflection pattern that resulted from a local deflection to be radially oriented, narrow, and confined to the vicinity of the probe. Specifically, he observed that the deflection did not spread along the BM in the longitudinal direction. Based on similar results from all cochlear turns, he concluded that the BM was minimally coupled. His report, however, did not state the range of BM deflections for which these results were obtained.

Recently, Naidu and Mountain (1998a, 1999) provided preliminary evidence for longitudinal coupling in the BM of the excised gerbil cochlea. The present study determines the response of an extended region of the cochlear turn to point deflections of the BM. The experiments were performed using a combination of local mechanical displacements and videomicroscopy. The data from these experiments were used to describe and quantify the coupling in the BM. Results from the three turns of the gerbil cochlea are presented and compared. The results show that the longitudinal coupling in the BM increases from base to apex. The potential impact of these results is studied using a one-dimensional model of the cochlea. The model simulations show that, at a given location, longitudinal coupling increases the effective stiffness of the OC near the characteristic frequency.

METHODS

Excised cochlear preparation

Experiments were performed on excised cochleae from mongolian gerbils (*Meriones unguicilatus*). The procedures were performed in accordance with guidelines provided by the Laboratory Animal Care Facility at Boston University. Female gerbils (30–50 g) were deeply anesthetized using a mixture of ketamine (0.16 mg/g) and xylazine (0.008 mg/g). Following decapitation, the temporal bones were rapidly excised and immersed in cold, oxygenated L-15 culture medium. Most of the bulla was removed to expose the cochlea.

The turn to be studied was carefully isolated. The cochlea was kept immersed in L-15 medium through out the isolation procedure. The bone above and below the turn of interest was gently scored to cut and separate the additional turns. The resulting preparation consisted of an entire cochlear turn with the inner spiral lamina, the outer spiral ligament, and the cochlear shell intact (Figs. 1A, D). During dissection, care was taken to leave Reissner's membrane (RM) intact in order to prevent accidental damage to the OC. The bony wall of scala tympani was opened in the vicinity of the measurement location to facilitate access to the underside of the BM.

Two groups of excised cochleae were prepared for study. In group I, RM was opened after the turn was isolated. The OC was then mechanically removed from the BM using a fine microhook. In group II, RM and the OC were left intact. The preparation resulting from either procedure was mounted in a petri dish, immersed in L-15 medium, and placed on the stage of an inverted microscope. The bottom of the petri dish was replaced by a cover slip to minimize refraction and loss of light entering the microscope objective.

Experimental paradigm

The OC was deflected from the underside of the BM using a piezoelectric probe (Olson and Mountain 1991) with a tip diameter of 10 μm (Fig. 1A). At the start of the experiment, the probe was advanced towards the BM using a motorized micromanipulator. The microscope was focused at the top of the BM and the measurement location was viewed using a CCD camera. In the camera view, the probe appeared as a dark shadow under the BM. The camera view was used to position the probe under the BM, within the medial pectinate zone (Fig. 1B) The probe was then advanced towards the BM until contact was established. Contact was determined visually and defined as the position when the movement of the probe resulted in just detectable movement of structures in the camera view. Following contact, the probe was advanced in 1 $-\mu$m increments to deflect the BM from 0 μm to a maximum of 15 μm. It was then retracted in 1 $-\mu$m increments from 15 μm, past 0 μm, to 4 $-\mu$m. This movement past the starting position was performed to enable the probe to completely detach from the BM at the end of each set of deflections. At each deflected position, an image of the BM was captured using a frame grabber card (Scion, AG5, Frederick, MD) and stored on a PC. At the end of the experiment, we obtained a

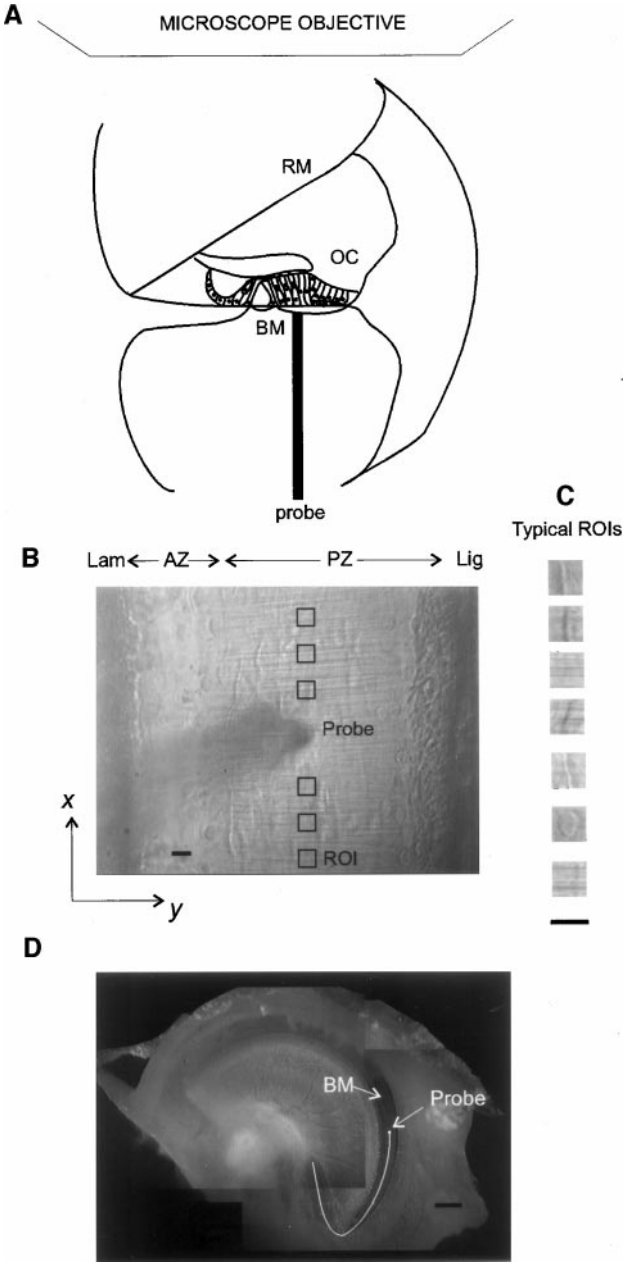

FIG. 1. **A**. Schematic drawing of the excised cochlear preparation showing the BM, OC, and RM. The probe is in contact with the BM and the measurement location is simultaneously viewed through the microscope objective. **B**. Microscope view of the BM showing the arcuate and pectinate zones (AZ, PZ), the osseous spiral lamina (LAM), the spiral ligament (LIG), and the probe. The squares represent regions of interest (ROI) that were used to study displacements along the turn. Scale bar = 10 μm. **C**. Typical ROIs chosen for study from several experiments. Scale bar = 10 μm. **D**. Reconstruction of the basal turn using multiple images. The white spot marks the position of the probe while the length of the white line represents the distance of the measurement location from the base of the cochlea. Scale bar = 250 μm.

family of images of the BM which corresponded to the deflection sequence.

The experiments described above were performed on cochlear preparations from both groups I and II. The properties of the BM alone were studied using preparations from group I. The properties of the BM with the OC present were studied using preparations from group II. The results from the two groups were then compared in order to determine the influence of the OC on the longitudinal coupling exhibited by the BM. In both experimental groups, data were collected from the three turns of the cochlea.

Position of experimental locations along the cochlea

The distance of each experimental location was measured with respect to the extreme base of the cochlea. Specifically, the length of the hook region of the BM was included in these measurements. Low-magnification images of the experimental location were digitized at the end of each experiment. These images were overlaid to reconstruct a composite image of the cochlear turn (Fig. 1D). In the low-magnification images, the probe typically appeared as a bright spot at the experimental location (Fig. 1D).

Distances were measured along the center line of the BM. For measurements in the basal turn, the entire distance could be determined from images obtained during a single experiment. Measurements in the second and third turns caused the other turns within the same cochlea to be damaged inevitably during removal. Therefore, the distances of these measurement locations from the base were measured by combining and aligning the composite image of the turn of interest with composite images of the missing turns reconstructed using images from other cochleae.

Image analysis

Structures in the plane of the microscope view exhibited radial and longitudinal displacements in response to vertical deflection of the BM by the probe. We refer to these displacements as *in-plane* displacements. The longitudinal coupling at the measurement location was characterized by studying the in-plane displacements of several well-defined morphological structures of interest as a function of their location along the cochlear turn. These displacements were determined by analyzing the images of the BM that were obtained for different probe deflections during the experiment.

Figure 2 outlines the procedure used to determine the displacement of a single structure on the BM in response to probe deflection. The structure of interest is represented by "S". The first column (Figs. 2A, B) shows a schematic drawing of the deflected BM for two vertical positions, Z_1 and Z_2, of the probe. The second column (Figs. 2C, D) represents the corresponding images of the BM that were digitized at these

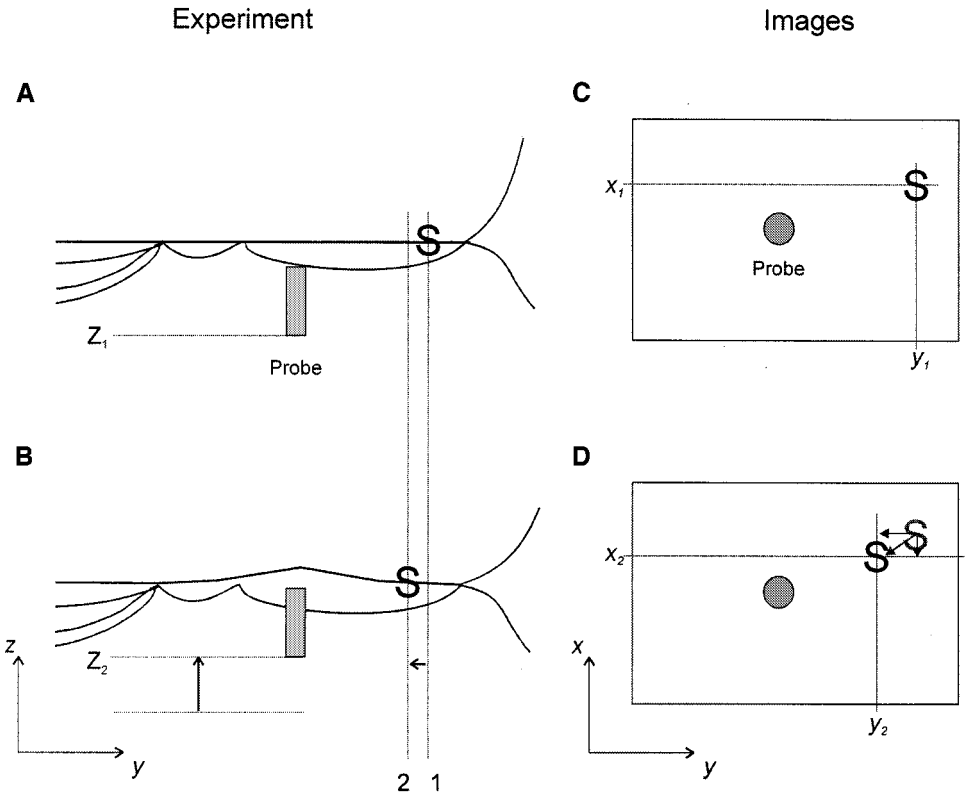

FIG. 2. Vertical deflection of the BM by the probe causes displacement of structures in the plane of the microscope view. The schematic diagrams on the left (**A, B**) show the BM deflected by the probe at two vertical positions. The motion of the structure S appears as a two-dimensional displacement across the corresponding digitized images (**C, D**). The magnitudes of the displacements have been exaggerated for clarity.

two instances during the experiment. When the probe is located at vertical position Z_1 (Fig. 2A), S is located at position 1 with coordinates (x_1, y_1) in the microscope view (Fig. 2C). When the probe moves vertically to position Z_2 (Fig. 2B), S moves to position 2 with coordinates (x_2, y_2) in the microscope view (Fig. 2D). The resulting displacements of S along the x and y are $\Delta x = x_1 - x_2$ and $\Delta y = y_1 - y_2$, respectively. The magnitudes of these displacements are obtained as follows. A region of interest (ROI) that encompasses the position of the structure of interest in both images is defined. This ROI is extracted from each image. The displacement of the structure is determined by cross-correlating the two ROIs.

Several ROIs were chosen for study. The ROIs were always arranged in a longitudinal array along the length of the cochlear turn (Fig. 1B). Typical ROIs from images from various experiments are shown in Figure 1c. The ROIs included both high-contrast edges of cells as well as fiber bundles. Therefore, the features within the ROIs yielded contrast boundaries that were multidirectional. The displacements in ROIs were computed using the images obtained as the probe retracted from the maximum deflection. This was done to ensure that the probe was in complete contact with the tissue and its movement was completely transferred to the BM. The ROIs were 32×32 square pixels in size. The size of each pixel was between 2.1 and 2.5 μm. Subpixel resolution was obtained by interpolating the pixels in the ROIs before correlation. This allowed the above analysis to measure displacements that were as small as 40 nm.

In the correlation technique, one image is shifted relative to the other until a maximum degree of overlap is achieved. This procedure inherently assumes that the structure of interest is displaced only in space and does not undergo a distortion in shape between the two images. In our experiments, this assumption was not valid when comparing images of the BM obtained for small probe deflections with those at large deflections. However, structures did preserve their shape reasonably well between images from adjacent probe deflections (an incremental deflection of 1 μm). Therefore, for each structure of interest, incremental displacements were first computed using images from adjacent probe deflections. The cumulative displacement of the structure in response to a given probe deflection from zero deflection was then determined by summing the corresponding incremental displacements.

RESULTS

Experiments were attempted in 28 excised cochleae. The results include pooled data that were successfully collected at 25 measurement locations in 23 cochlear preparations. Measurements could not be performed

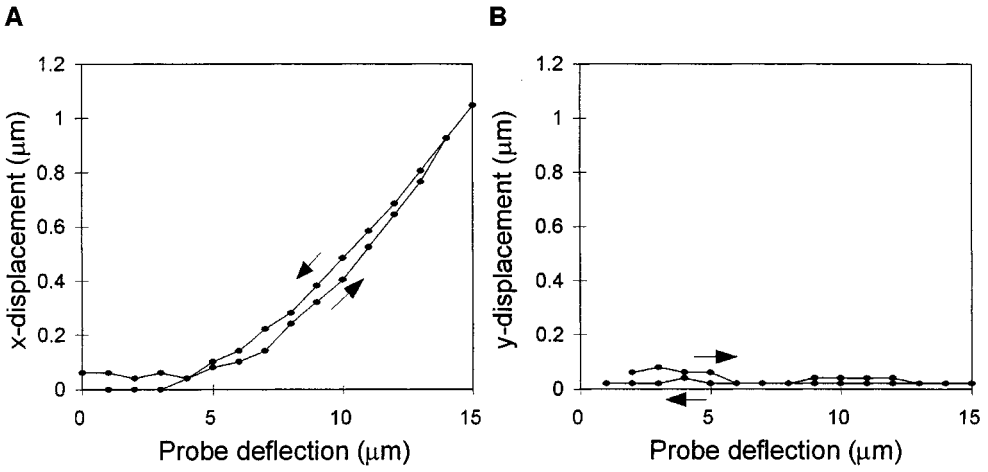

FIG. 3. Magnitude of displacements within a single ROI plotted as a function of distance from the probe. The arrows indicate the direction of probe movement. **A**. x-displacement. **B**. y-displacement.

in the remaining 5 cochleae as the turn of interest was damaged during isolation.

Structural features of the basilar membrane

A typical digitized image of the BM is shown in Figure 1B. The *x* axis coincides with the longitudinal direction along the length of the cochlea, and the *y* axis coincides with the radial direction from spiral lamina to spiral ligament. Several structural characteristics of the BM can be identified in the image. The medial and lateral edges of the BM and their respective attachments to the spiral lamina and spiral ligament are visible. Anatomically, the BM may be divided into two regions (Iurato 1962). The pectinate zone can be identified by the regular, radial, and parallel arrangement of fiber bundles. The arcuate zone, in contrast, appears relatively homogeneous. Here, the bundles separate into individual fibers that lie side by side before they subsequently enter the spiral lamina. Spindle-shaped tympanic cells oriented along the cochlear spiral (Slepecky 1997) are visible in the pectinate zone. During experiments, the probe appears as a dark shadow under the medial pectinate zone.

Displacements in ROIs as a function of probe deflection

The image analysis technique was used to determine the *x* and *y* components of the displacement within each ROI. Figure 3 shows the relative magnitudes of these displacements within a typical ROI. The *x* component (longitudinal direction) of the displacement (Fig. 3A) is significantly larger than the *y* component (radial direction of the displacement (Fig. 3B). This result is expected since the probe deflection would cause structures along the BM to move toward the probe itself. Since the ROIs of interest were chosen to lie in a longitudinal array in line with the position of the probe (Fig. 1B), the corresponding displacements are expected to be along the *x* direction.

Figures 4A and B show the displacements in several ROIs plotted as functions of ROI distance from the probe. Each curve is a displacement profile that represents the displacements in all of the ROIs for a single probe deflection. Therefore, a family of displacement profiles is obtained for the entire deflection sequence. Since the displacement in each ROI is predominantly along the *x* direction, we have restricted our discussion of the results from the ROIs to the *x* component of the measured displacements.

The *x* component of the displacement profile decreased with increasing distance from the probe. This decrease with distance was quite symmetric, irrespective of whether the ROIs were located apically or basally along the cochlea, with respect to the probe. Therefore, in the rest of the discussion of the data, only one side of the displacement profile will be presented. In general, it was difficult to obtain data from structures located in the vicinity of the probe. This region had poor contrast due to the shadow caused by the probe (Fig. 1B). Therefore, it was not possible to select ROIs that contained well-defined structures in order to reliably apply the image analysis technique.

Displacement profile shape is independent of BM vertical deflection

Displacement profiles were generated for probe deflections up to 15 μm (Fig. 4A). In order to assess whether the shape of the displacement pattern changed with increasing BM deflection, the profiles were normalized by the maximum displacement obtained for each deflection. It was assumed that the displacement at a given location was proportional to the vertical deflection of the BM at the same location. Figure 4C shows that the curves overlap as a result of this normalization procedure. This result indicates

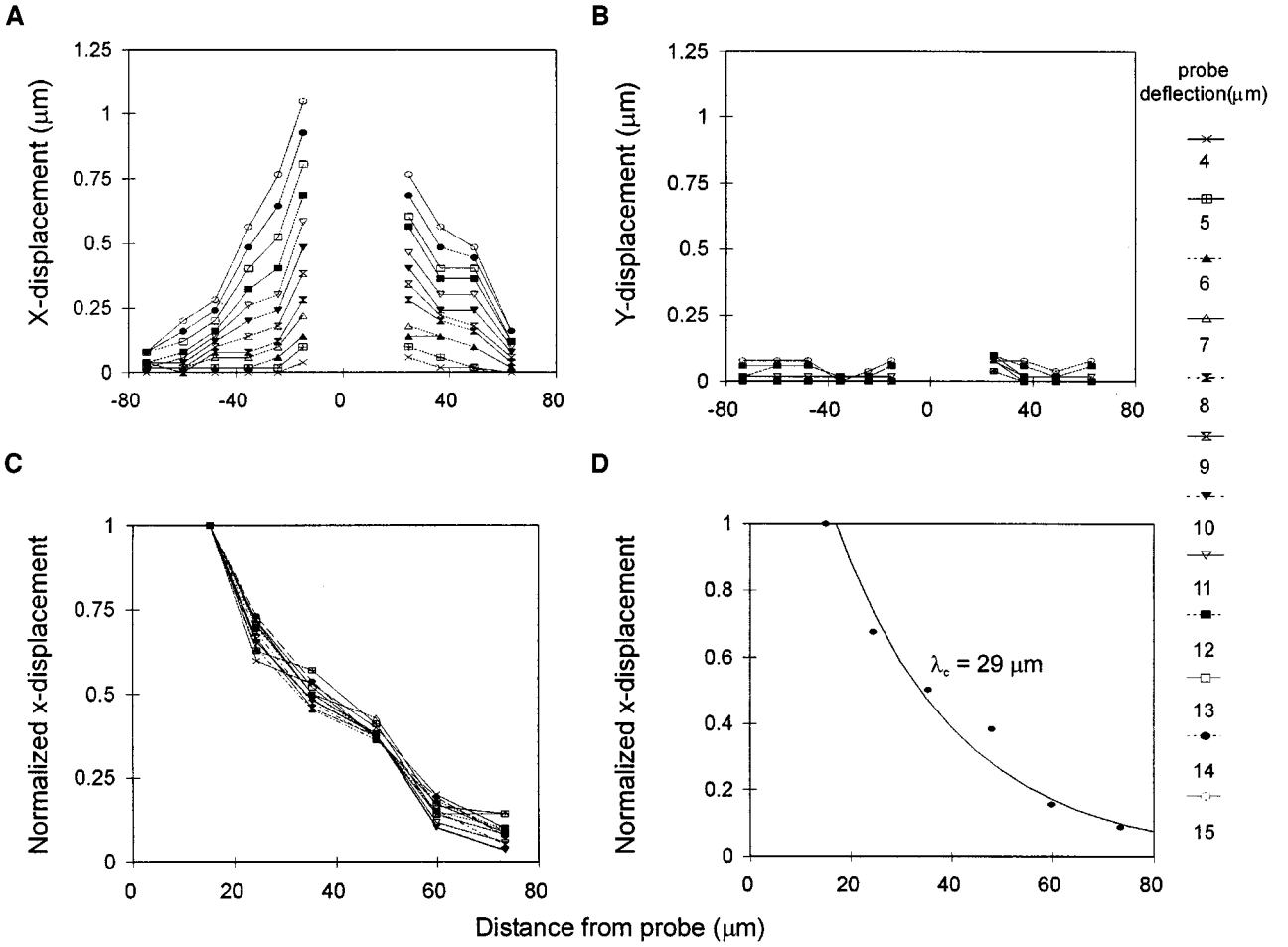

FIG. 4. Magnitude of displacements on ROIs along the BM plotted as a function of distance from the probe, for several probe deflections. **A**. *x* displacements decrease symmetrically with increasing distance on either side of the probe. **B**. *y* displacements are small over the entire range of probe deflections. **C**. *x* displacement profiles from **A**, normalized by the displacement closest to the probe, for several probe deflections. **D**. Normalized data was fit using Eq. (1) with $R^2 = 0.97$.

that the profile shape is independent of BM vertical deflection.

Quantitative measure of longitudinal coupling

In the final step in the analysis procedure, a quantitative measure of the longitudinal coupling was determined for the measurement location. This was obtained using the normalized displacement profile (Fig. 4C). The normalized profiles obtained for probe deflections between 5 and 15 μm were averaged together. The averaged, normalized, probe-elicited displacement Δx with increasing distance x from the probe was then fit using the exponentially decaying function

$$\Delta x = Ce^{-z/\lambda_c} \qquad (1)$$

where C is a constant and λ_c is the space constant that describes the rate at which the displacement falls with distance from the excitation location. The space constant λ_c was chosen to represent the longitudinal coupling at each location. By definition, this value determines the distance along the cochlear spiral over which the displacement falls from the maximum to 37% of the maximum value. Figure 4D shows the fit to normalized data obtained from Figure 4C.

The influence of the organ of Corti

The effect of the OC on BM coupling was studied by comparing results from experiments in which the OC was removed from the BM (group I) with those in which the OC was left intact (group II). Figure 5 compares the normalized displacement profiles obtained from experiments in the two groups that were performed at similar locations in the second turn. The open circles represent the data from the BM alone, while the filled circles represent the data obtained from the BM with the OC intact. The lines represent

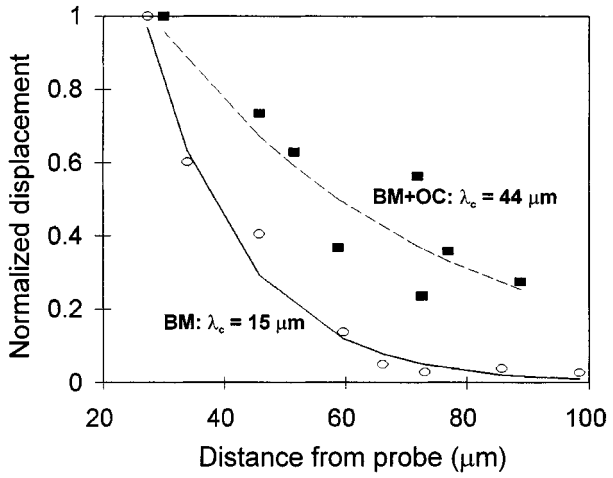

FIG. 5. Displacement profile for the BM alone (8.29 mm from base) compared with that for the BM with the OC present (8.33 mm from base). The space constants describe the exponential fits to the data using Eq. (1). R^2 for fits: BM: 0.92, BM + OC: 0.73.

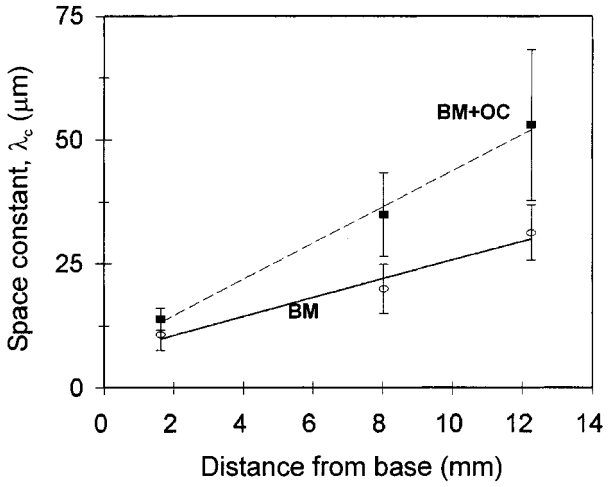

FIG. 6. Average space constants λ_c determined at three locations along the cochlea. The error bars represent the corresponding standard deviations characterizing the data at each location. The lines represent linear regression fits to the data used to describe the variation of the space constants with distance along the cochlea [see Eqs. (2) and (3)].

TABLE 1

Variability of space constants across experiments[a]

	BM			*BM + OC*		
Mean distance from base (mm)	*mean (μm)*	*SD*	*N*	*mean (μm)*	*SD*	*N*
1.6	12.9	3.7	4	16.7	1.9	5
8.1	19.7	4.8	4	34.5	8.5	5
12.3	33.3	3.4	3	56.9	14.7	4

[a]Mean and standard deviation (SD) were determined for three locations along the cochlea. *N* represents the number of successful experiments that were performed at each measurement location.

fits to each of the data sets using Eq. (1). The displacements decrease more gradually when the OC is present. A comparison of the values of λ_c determined for these two experiments shows that the space constant obtained for the BM with the OC present, is larger than that obtained for the BM alone. This indicates that, at a given location along the cochlea, the cells of the OC increase the overall coupling exhibited by the BM.

The space constants were compared for different measurement locations along the cochlea. These results are summarized in Table 1. Representative values of λ_c were obtained at three locations (Fig. 6). These values were determined by averaging the space constants obtained from multiple experiments that were performed at similar locations. These experimental locations differed at most by 500 μm across animals. The lines represent linear regression fits that were used to determine the variation of the space constants as a function of measurement location x along the cochlea. The following expressions describe the fits that were obtained:

$$\text{BM alone: } \lambda_c = 8.5 + 1.8x \quad (2)$$

$$\text{BM + OC: } \lambda_c = 9.0 + 3.7x \quad (3)$$

where λ_c is in units of μm while x is in units of mm. In both cases, λ_c increased monotonically from base to apex. When the cells were present, the coupling was consistently greater than that determined for the BM alone. Furthermore, this effect was larger in the apex than in the base.

DISCUSSION

In the excised cochlear preparation, all of the scalae are uniformly bathed in culture medium. The resulting altered ionic composition in scala media is no longer similar to that of endolymph within the intact cochlea. Such a situation could potentially alter the properties of the OC. However, we have previously shown that the measured stiffness of the OC in this preparation of the gerbil cochlea agrees well with measurements *in situ* (Naidu and Mountain 1998b). Besides, the measured stiffness remains stable for about three hours following surgery. This indicates that the underlying mechanical properties of the BM and OC do not change during this period. Since BM longitudinal coupling results from these mechanical properties, we believe that our results obtained from the excised cochlea are representative of the cochlea *in situ*.

The displacements within each ROI are calculated by summing incremental displacements that are produced by each micrometer of probe deflection. As a

result, an error in the calculation of a single incremental displacement at the beginning of the deflection sequence can propagate through the rest of the displacement profile. Figure 3A shows the deflection profile that was determined within a typical ROI. Because of propagating errors, the displacements calculated for small forward deflections of the probe are different from those calculated as the probe was retracting back. However, the difference in the calculated deflections corresponds to a fraction of a pixel. The displacements that were used in the calculations were typically many pixels in magnitude. Therefore, we assume that our subsequent calculations are not significantly affected by such incremental errors.

Figure 3 shows that the displacement within the ROI is not zero for zero probe deflection. This is because the measured deflection of the probe is not identical to the true vertical deflection of the BM. It is difficult to accurately define the zero deflection position of the probe. We have determined this starting position by focusing the microscope to the top of the BM and visually detecting the movement of structures in the microscope view as the probe advances toward the BM. However, this method can be influenced by the movement of structures that lie out of the plane of focus. Such movement causes errors in the determination of the starting location of the probe. As a result, contact may occur before structures in the plane of focus begin to move. To circumvent this problem, we have assumed that the in-plane displacement at a given location on the BM is proportional to the true vertical deflection at the same location. The maximum in-plane deflection measured close to the probe is then proportional to the true vertical deflection of the BM near the probe. Therefore, by normalizing our data by the maximum in-plane displacement measured within each displacement profile, we are normalizing the data by a value that is proportional to the true vertical deflection of the BM. This prevents the errors that would be introduced if the measured probe deflections were used to normalize the data.

Longitudinal coupling was characterized for BM deflections in the range of 1–15 μm. In contrast, *in vivo* measurements indicate that the vertical deflection of the BM at the characteristic frequency place of a pure tone is only of the order of a few nanometers at low sound levels (Robles et al. 1986). Our results show that the shape of the displacement profile is independent of BM deflection (Fig. 4C). We therefore believe that the same profile shape would result from vertical deflections of the BM in the nanometer range.

BM morphology shows clear differences between the arcuate and pectinate zones. Miller (1985) suggested that these two regions could exhibit differing amounts of longitudinal coupling. In this study, it was not possible to characterize longitudinal coupling in the arcuate zone. The image analysis technique that was used may be applied effectively only to ROIs that contain distinct features. While the pectinate zone contains high-contrast edges and fiber structure, the arcuate zone has poor contrast because of its homogeneous appearance. This lack of contrast hindered the selection of ROIs suitable for the study of longitudinal coupling in the arcuate zone.

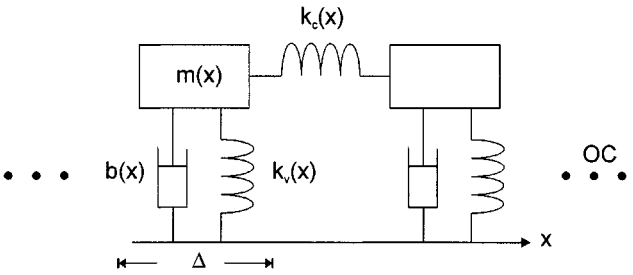

FIG. 7. BM model used to study the effect of longitudinal coupling. Each section has width Δ and is characterized by a mass $m(x)$, stiffness $k_v(x)$, and damping $b(x)$ per unit length. $k_c(x)/\Delta$ represents the longitudinal coupling between adjacent sections.

Our study demonstrates that the BM exhibits longitudinal coupling that increases from base to apex. Though direct, quantitative comparisons with previous studies are not possible, our results are qualitatively similar to the results described by von Békésy (1960). We did not observe results similar to those described by Voldřich (1978). The deflection profile described by Voldřich was limited to the width of the probe. His result suggested that the BM may be represented by a series of independent beams. In contrast, we observed a gradual decrease in displacement with distance from the probe. From a structural mechanics perspective (Timoshenko and Woinowsky-Kreger 1959), our results indicate that the BM deflects like a plate in response to a local deflection. In such a representation, the effective length of the plate would be a function of longitudinal coupling in the BM.

Does the spatially varying longitudinal coupling have significant implications for cochlear mechanics? We studied the effect of longitudinal coupling on the motion of the OC using a one-dimensional model (Fig. 7). The results are described in Appendix A and indicate that the effective stiffness of the OC is proportional to the factor $[1 + (2\pi\lambda_c/\lambda)^2]$, where λ is the wavelength of the traveling wave. Therefore, longitudinal coupling would cause an tangible increase in the effective stiffness when the factor $2\pi\lambda_c/\lambda$ is not negligible when compared with unity.

The increase in effective stiffness was calculated at two locations along the gerbil cochlea where the wavelength of the traveling wave has been determined or could be estimated at the characteristic frequency (CF). The wavelength at the 18-kHz location at the base of the cochlea has been determined to be ~130

TABLE 2

Increase in effective BM stiffness near CF as a result of longitudinal coupling at two locations along the cochlea

Distance from base (mm)	*CF (kHz)*	*λ[a] (μm)*	*λ_c[b] (μm)*	*$(2\pi\lambda_c/\lambda)$*	*$\Delta k = (2\pi\lambda_c/\lambda)^2 \times 100$[c] (%)*
3.2	18	130	20.8	1.00	100.00
9.4	1.3	590	43.7	0.46	21.16

[a] λ is the wavelength of the traveling wave near CF.
[b] λ_c is the space constant determined for the BM + OC using Eq. (3).
[c] Δk is the percentage increase in the effective stiffness of the OC.

μm [Ren, personal communication, based on Ren (2001) and Ren and Nuttall (2000)]. The wavelength at the 1.3-kHz region near the apex was estimated using reverse correlation functions from low-frequency auditory nerve fibers (Carney and Friedman 1996; Carney, unpublished) to be ~590 μm (see Appendix B). At the locations of interest, the space constant λ_c was estimated for the BM with the OC present using Eq. (3).

Longitudinal coupling can cause a significant increase in the effective stiffness of the OC near CF. Table 2 shows the factor $2\pi\lambda_c/\lambda$ and the corresponding increase in effective stiffness for the two locations considered. At the base, the effective stiffness is increased by ~100%. At the apex, the effective stiffness is increased only by ~20%. These results indicate that longitudinal coupling cannot be neglected when the wavelength is small and that coupling is expected to exert a greater influence on the motion of the OC at the base than at the apex.

The wavelength of the traveling wave shortens as it approaches its characteristic place (von Békésy 1960). For frequencies less than CF, the wavelength is large and the factor $2\pi\lambda_c/\lambda$ would be a negligible fraction when compared with unity and the corresponding increase in the effective stiffness would be very small. Therefore, longitudinal coupling is not expected to influence the motion of the BM for frequencies less than CF.

The results from our study show that the BM, both with and without the OC, is longitudinally coupled. The space constant that describes the longitudinal coupling in the BM increases from base to apex. Model simulations show that longitudinal coupling increases the effective stiffness of the OC when the wavelength of the traveling wave is small. Longitudinal coupling is, therefore, expected to influence the motion of the OC for frequencies close to CF.

ACKNOWLEDGMENTS

Laurel Carney generously provided the reverse-correlation functions for numerous auditory nerve fibers. Tianying Ren provided us with data from Ren and Nuttall (2000) and Ren (2001). We appreciate the comments and suggestions provided by Allyn Hubbard, Dennis Freeman, Domenica Karavitaki, and the reviewers on the initial manuscript. This research was supported by NIDCD.

APPENDIX A

The effect of longitudinal coupling on OC displacement

The effect of longitudinal coupling on OC displacement was studied using a one-dimensional model of the OC. The model is shown in Figure 7. For convenience, the OC is divided into several sections of width Δ. The parameters $m(x)$, $k_v(x)$, and $b(x)$ represent the mass, stiffness, and damping per unit length of the OC. In the absence of longitudinal coupling, the force F developed in a single section as a result of its stiffness in response to a vertical deflection $z(x)$ is given by

$$F = k_v \, \Delta \, z(x) \tag{4}$$

BM longitudinal coupling is represented by an additional stiffness $k_c(x)$ between adjacent sections. While $k_v(x)$ is defined in N/m^2, it is convenient to define $k_c(x)$ in units of N. These units define a compliance per unit length of the OC. It is assumed that $k_c(x)$ responds only to relative vertical deflections between sections. The force per unit length developed due to stiffness is

$$\frac{F}{\Delta} = k_v z(x) + \frac{k_c}{\Delta^2}\left[-z(x+\Delta) + 2z(x) - z(x-\Delta)\right] \tag{5}$$

As the width of each section becomes small, Eq. (5) may be rewritten as

$$\frac{dF}{dx} = \left[k_v z(x) - k_c \frac{\partial^2 z(x)}{\partial x^2}\right] \tag{6}$$

The results from the present study show that step deflections of the BM generate an in-plane displacement profile Δx that decreases exponentially with distance along the cochlea, from the site of excitation [see Eq. (1)]. It is asssumed that Δx is a scaled representation of the corresponding vertical deflection profile

at each location. The solution for $z(x)$ can then be obtained from Eq. (1) in the form

$$z(x) = A_1 e^{-x/\lambda_c} \tag{7}$$

where A_1 is a constant. In order to determine the relationship between λ_c, $k_v(x)$, and $k_c(x)$, consider the solution to Eq. (6) at a section located away from the excitation. Substituting Eq. (7) in Eq. (6), with $dF/dx = 0$,

$$0 = k_v A_1 e^{-x/\lambda_c} - k_c \frac{A_1}{\lambda_c^2} e^{-c/\lambda_c} \tag{8}$$

from which

$$\lambda_c^2 = \frac{k_c}{k_v} \tag{9}$$

We can now calculate the pattern of OC displacement in response to sound stimulation. The traveling wave generated by a pure-tone stimulus generates sinusoidal motion along the length of the OC (von Békésy 1960). The wavelength of the traveling wave decreases as it approaches the characteristic place. At a given instant in time, the local deflection pattern around the characteristic place may be approximated by the sinusoid

$$z(x) = A_2 \sin\left(\frac{2\pi x}{\lambda}\right) \tag{10}$$

where A_2 is the amplitude and λ is the wavelength of the traveling wave. From Eq. (6), the force per unit length due to the stiffness is

$$\frac{dF}{dx} = \left[k_v A_2 \sin\left(\frac{2\pi}{\lambda}x\right) + k_c A_2 \left(\frac{2\pi}{\lambda}\right)^3 \sin\left(\frac{2\pi}{\lambda}x\right)\right] \tag{11}$$

so that

$$\frac{dF}{dx} = \left[1 + \frac{k_c}{k_v}\left(\frac{2\pi}{\lambda}\right)^2\right] k_v A_2 \sin\left(\frac{2\pi}{\lambda}x\right) \tag{12}$$

Substituting Eq. (9) into Eq. (12),

$$\frac{dF}{dx} = \left[1 + \left(\frac{2\pi\lambda_c}{\lambda}\right)^2\right] k_v A_2 \sin\left(\frac{2\pi}{\lambda}x\right) \tag{13}$$

From Eq. (13), the effective stiffness of the section is proportional to $[1 + (2\pi\lambda_c/(\lambda)^2]$. When $(2\pi\lambda_c/\lambda)$ is not negligible when compared with unity, the effective stiffness will increase as a result of longitudinal coupling.

APPENDIX B

Estimation of traveling wave wavelength

The wavelength, λ, close to CF may be estimated from the phase, $\varphi(x)$, of the traveling wave as a function of position, x, along the cochlea using the expression

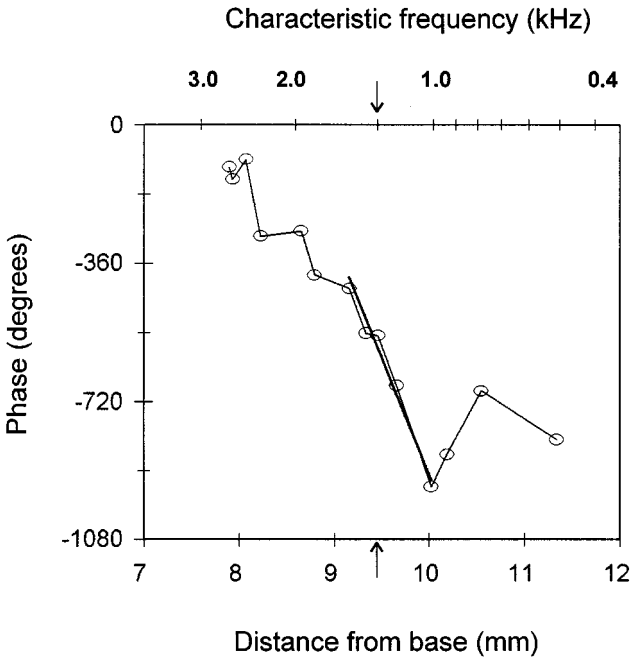

FIG. 8. Phase of the traveling wave $\varphi(x)$ as a function of position along the cochlea for a 1.3-kHz input frequency, estimated using reverse-correlation functions from low-frequency auditory nerve fibers. The x axis (linear scale) at the bottom of the figure describes the locations along the basilar membrane (in mm) innervated by each of the corresponding nerve fibers. The corresponding CFs at these locations are indicated on the x axis (log scale) at the top of the figure. Arrows on both x axes indicate the location 9.4 mm from the base (CF = 1.3 kHz). The bold line represents the linear regression fit to the phase data around this location. This fit was used to determine the slope of the phase–position function.

$$\lambda = 2\pi \Big/ \left|\frac{d\varphi(x)}{dx}\right|_{x\mathrm{CF}} \tag{14}$$

where x(CF) represents the distance of the characteristic place of the CF of interest along the length of the cochlea.

To estimate the wavelength at the apex, a phase–position plot was first constructed around the region tuned to 1.3 kHz using reverse-correlation functions from a population of gerbil auditory nerve fibers (Carney and Friedman 1996; Carney, unpublished). The magnitude and phase of the reverse-correlation function for a fiber tuned to a given CF was assumed to represent the response of the BM at the corresponding innervation site. The position of each innervation site along the cochlea was determined from the fiber CF using the frequency-place map of the gerbil (Müller 1996). Next, the phase of the response of each fiber at 1.3 kHz was determined. The phase–position plot was then created by plotting this phase, determined for each fiber, against the position of the corresponding innervation site (Fig. 8). The resulting function was unwrapped with position along the cochlea, relative to the phase at the 1.3-kHz characteristic place (9.4

mm from base) to be consistent with the accumulating phase of the traveling wave, i.e., the phase accumulated at locations basal to the 1.3-kHz characteristic place was assumed to be smaller than the phase accumulated at locations apical to it. A linear regression line was fit to the data around the 9.4-mm location. The number of data points to be included in the fit were determined using the 10-dB bandwidth of the reverse-correlation function for the 1.3-kHz fiber. This 10-dB bandwidth was ~500 Hz. It was converted, using the frequency–place map, to an approximate distance of 1 mm centered around the 1.3-kHz place. Therefore, the fit included only data points that lay within 0.5 mm on either side of the 9.4 mm location. The slope of the regression line was used to represent the slope of the phase–position plot at the 1.3-kHz characteristic place. The wavelength was then calculated using Eq. (14).

REFERENCES

ALLEN JB, SONDHI MM. Cochlear macromechanics: time domain solutions. J. Acoust. Soc. Am. 66:123–132, 1979.

CARNEY LH, FRIEDMAN M. Nonlinear feedback models for the tuning of auditory nerve fibres. Ann. Biol Med. Eng. 24:440–450, 1996.

DE BOER E. Mechanics of the Cochlea: Modeling Efforts. In: Dallos P, Popper AN, Fay RR, (eds) The Cochlea. Springer-Verlag, New York, 1997, pp. 258–317.

IURATO S. Functional implications of the nature and submicroscopic structure of the tectorial and basilar membranes. J. Acoust. Soc. Am. 34:1386–1395, 1962.

MILLER CE. Structural implications of basilar membrane compliance measurements. J. Acoust. Soc. Am. 77:1465–1474, 1985.

MÜLLER M. The cochlear place-frequency map in the adult and developing gerbil. Hear. Res. 94:148–156, 1996.

NAIDU RC, MOUNTAIN DC. (1998a) Can longitudinal coupling within the organ of Corti be neglected? Assoc. Res. Otolaryngol. 21:718.

NAIDU RC, MOUNTAIN DC. Measurements of the stiffness map challenge a basic tenet of cochlear theories. Hear. Res. 124:124–131, 1998b.

NAIDU RC, MOUNTAIN DC. Longitudinal coupling within the basilar membrane and reticular lamina. Symposium on Recent Developments in Auditory Mechanics, abstract 26M05, World Scientific Publishing, Singapore, 1999.

OLSON ES, MOUNTAIN DC. In vivo measurement of basilar membrane stiffness. J. Acoust. Soc. Am. 89:1262–1275, 1991.

REN T. Direct measurement of the traveling wave using a scanning laser interferometer in sensitive gerbil cochlea. Assoc. Res. Otolaryngol. 24:555, 2001.

REN T, NUTTALL A. Measurement of the basilar membrane vibration at the basal turn in sensitive gerbil cochlea. Assoc. Res. Otolaryngol. 23:717, 2000.

RHODE WS. An investigation of postmortem cochlear mechanics using the Mössbauer effect. Møller AR, Basic Mechanisms in Hearing. Academic New York, 1973, pp. 49–63.

ROBLES L, RUGGERO MA, RICH NC. Basilar membrane mechanics at the base of the chinchilla cochlea. I. Input –output functions, tuning curves and response phase. J. Acoust. Soc. Am. 80:1364–1374, 1986.

SLEPECKY N. Structure of the mammalian cochlea. Dallos P, Popper AN, Fay RR, The Cochlea. Springer-Verlag, New York, 1996, 44–129.

TIMOSHENKO S, WOINOWSKY-KREGER S. Theory of Plates and Shells. McGraw-Hill, New York, 1959.

VOLDŘICH L. Mechanical properties of the basilar membrane. Acta Otolaryngol. 86:331–335, 1978.

VON BÉKÉSY G. Experiments in Hearing. McGraw-Hill, New York, 1960.

WICKESBERG RE, GEISLER CD. Longitudinal stiffness coupling in a 1-dimensional model of the peripheral ear. In: Allen JB, Hall JL, Hubbard A, Neely ST, Tubis A, (eds) Peripheral Auditory Mechanisms. Springer-Verlag, Berlin, 1986, pp. 113–120.